Available online at www.sciencedirect.com

ScienceDirect

Ceramics International 40 (2014) 2127–2133

CERAMICS INTERNATIONAL

www.elsevier.com/locate/ceramint

CuO nanobelts synthesized by a template-free hydrothermal approach with optical and magnetic characteristics

Reda M. Mohamed[a,b], Farid A. Harraz[b,c,*], Ahmed Shawky[b]

[a]*Chemistry Department, Faculty of Science, King Abdulaziz University, P.O. Box 80203, Jeddah 21589, Saudi Arabia*
[b]*Nanostructured Materials and Nanotechnology Division, Central Metallurgical Research and Development Institute (CMRDI), P.O. Box 87 Helwan, Cairo 11421, Egypt*
[c]*Promising Centre for Sensors and electronic Devices (PCSED), Advanced Materials and Nano-Research Centre, Najran University, P.O. Box 1988, Najran 11001, Saudi Arabia*

Received 10 July 2013; received in revised form 25 July 2013; accepted 26 July 2013
Available online 2 August 2013

Abstract

The present study reports a simple hydrothermal approach for conveniently synthesizing cupric oxide (CuO) nanobelts without a templating agent. Electron microscopic studies indicate that these nanobelts have a wide stem (300–500 nm) and sharp tip (80–150 nm), with lengths up to 6 μm. X-ray diffraction patterns confirm the formation of a single monoclinic phase of CuO. A possible reaction mechanism was proposed to account for the growth of nanobelts. The optical properties of the products were investigated using UV–vis spectroscopy and photoluminescence (PL) measurement. The direct band gap energy for CuO nanobelts was estimated to be 3.2 eV, which is larger than the value of bulk CuO and likely related to quantum size effects. The magnetic properties of CuO nanobelts measured at room temperature exhibited a ferromagnetic behavior with a coercive force (*Hc*) of 93.35 Oe, whereas a paramagnetic behavior was observed in liquid nitrogen. The magnetic behavior was discussed in terms of CuO morphology effects.

Keywords: A. Powders: chemical preparation; B. Electron microscopy; C. Magnetic properties; C. Optical properties

1. Introduction

During the last decade, great attention has been paid to the synthesis and development of nanoscale inorganic materials due to its novel physico-chemical properties that are often observed as opposed to the corresponding bulk materials [1–7]. Metal oxide nanostructures are versatile class of materials that stimulated great interests for scientists and have vast industrial applications [8,9]. A cost-effective technique to synthesize oxide nanopowders with controlled size and morphology, crystallinity, and phase selectivity remains a challenge to material scientists [10]. This is particularly true for cupric oxide (CuO) nanostructures, which have recently received considerable attention due to their fundamental and practical importance. CuO is a *p*-type semiconductor with narrow band gap energy (1.2 eV) [11]. Owing to its unique physicochemical properties, the material has a wide range of applications in, for example, gas sensors [12], solar energy conversion [13], catalysis [14], magnetic storage media [15], high critical temperature superconductors [16], optical switches [17], lithium batteries [18,19] and as electrode materials for capacitors [20]. In addition, previous studies reported three magnetic phases for CuO that may form the basis for several high-*Tc* superconductors and as a giant magnetoresistance material [21–23].

Several methods have been developed to synthesize one-dimensional (1D) CuO nanostructures, including chemical vapor deposition (CVD) [24], electrochemical technique [25], laser vaporization [26], and hydrothermal treatment [19,27,28]. However, to date, there are challenges in controlling the size and morphology, crystallinity, and unidirectional growth of as-synthesized material. Among the abovementioned methods,

*Corresponding author at: Nanostructured Materials and Nanotechnology Division, Central Metallurgical Research and Development Institute (CMRDI), P.O. Box 87 Helwan, Cairo 11421, Egypt. Tel.: +20 2 25010 640; fax: +20 2 25010 639.
E-mail addresses: fharraz68@yahoo.com, fharraz@cmrdi.sci.eg (F.A. Harraz).

0272-8842/$ - see front matter © 2013 Elsevier Ltd and Techna Group S.r.l. All rights reserved.
http://dx.doi.org/10.1016/j.ceramint.2013.07.129

the hydrothermal technique is considered one of the most promising routs to synthesize nanomaterials with various structures and morphologies at a relatively low temperature and in mild conditions [29–31]. In this study, we report a simple hydrothermal method to synthesize CuO nanobelts. To better understand the conditions necessary for nucleation and growth of CuO nanostructures using a similar method as that proposed by Du et al. [32], a detailed investigation was conducted in which the phase and morphology of nanostructured CuO are correlated to its structural, optical, and magnetic properties.

The aim of the present work is to provide a solid base of knowledge for the hydrothermal synthesis of CuO semiconducting nanostructures that exhibit optical activity and ferromagnetic properties. The ability to fabricate single-phase CuO nanostructures with controlled morphology would principally enrich our understanding of CuO's fundamental properties and open the door toward its possible applications. To achieve this objective, the structural analysis and morphology of the as-synthesized CuO product were characterized by XRD, FT-IR, SEM, EDS, and TEM. Optical properties were also evaluated using UV–vis and PL measurements. Furthermore, magnetic properties were examined using VSM at room temperature and in liquid nitrogen. The reaction mechanism involved during the hydrothermal treatment was also discussed.

2. Experimental

All chemical reagents are of analytical grade and used without further purification. In a typical synthesis procedure, 1 g $Cu(NO_3)_2$ is dissolved in 100 ml of deionized water, followed by adding a 30 ml ammonia solution ($NH_3 \cdot H_2O$) under constant stirring. The pH of the above solution is adjusted at 9.5 by adding 1 M NaOH solution dropwise, until a blue precipitate of $Cu(OH)_2$ is formed. The precipitate is then filtered and washed several times using water to remove the un-reacted matter. Next, the solid product is dissolved in 50 ml of deionized water and transferred into a Teflon-lined stainless autoclave. The autoclave is subsequently put into an oven and kept at 80, 100, 120, 130, or 140 °C for 20 h. The autoclave was left to cool naturally at room temperature. The black solid product was separated by centrifugation, washed several times with de-ionized water, and dried at 80 °C. A flow chart describing the main steps employed during the hydrothermal method is depicted in Fig. 1.

Phase identification was performed by X-ray diffraction (XRD, Bruker axs D8 Advance, Germany) with Cu-kα radiation ($\lambda = 1.5406$ Å). Measurements were taken with a tube power of 40 kV and 40 mA, from 10 to 80° 2θ, with a 0.02° 2θ step size and 0.4 s count time. For morphological and structural analysis, a JEOL JEM-1230 transmission electron microscope (TEM) operating at 200 kV was used to record the selected-area electron diffraction (SAED) patterns. Before TEM observation, samples were prepared by dispersing a trace amount of the powder in ethanol followed by ultrasonic vibration for 20 min. A carbon film coated copper grid was quickly immersed into the dispersion and left in air to dry. The as-synthesized sample was imaged by scanning electron microscopy (SEM, JSM-5400), coupled with energy dispersive X-ray spectroscopy (EDS) for chemical identification. FT-IR spectra were measured using a 3600 JASCO spectrophotometer. The spectra were collected over the frequency range of 4000 to 400 cm^{-1}. UV–vis spectroscopy measurements (V570 spectrophotometer Jasco Co) were performed. Photoluminescence was measured at room temperature via a spectrofluorophotometer, SHIMATDZU RF-5301PC, using a 150 W xenon lamp as an excitation source. The magnetic properties of the samples were measured at room ($T = 298$ K) and liquid N_2 ($T = 77$ K) temperature with a vibrating sample magnetometer (VSM, LDJ 9600-1, USA) in an applied field of ~12 kOe.

3. Results and discussion

3.1. Structural analysis and morphology

X-ray diffraction characterization of CuO nanostructures synthesized at different hydrothermal temperatures is given in Fig. 2(a), and the EDS chemical analysis is shown in Fig. 2(b). Phase identification indicates that the as-formed samples are pure CuO. No other impurity peaks were detected, indicating the high purity of the samples. All diffraction peaks can be perfectly indexed to a monoclinic CuO phase with the following cell constants: $a = 4.69$ Å, $b = 3.42$ Å, and $c = 5.13$ Å (JCPDS card no. 80-1916). The peaks with 2θ values of 32.52°, 35.58°, 38.84°, 48.88°, 53.52°, 58.51°, 61.64°, 66.23°, 68.10°, 72.55°, and 75.27° correspond to the crystal planes of 110, −111, 111, −202, 020, 202, −113, 022, 220, 311, and 004 of crystalline CuO, respectively. The peak intensities and

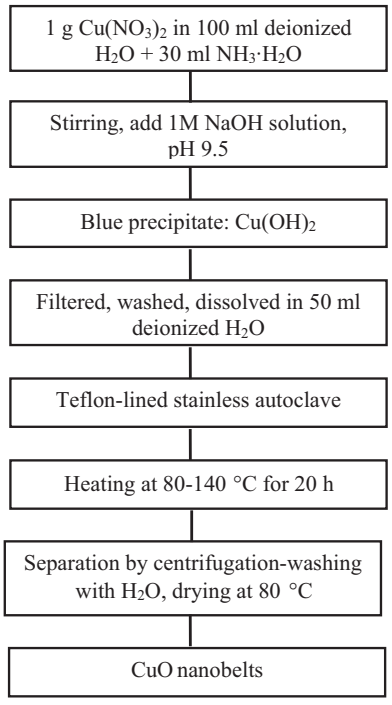

Fig. 1. Schematic flowchart for the preparation of CuO nanostructures via a hydrothermal technique.

widths clearly imply that the samples are highly crystalline. The reflection peak positions are not shifted but the shapes are broader than the standard peaks of CuO, which is essentially attributed to the small size of as-synthesized CuO nanostructures. With the increase of hydrothermal temperature from 80 to 140 °C, the diffraction peaks become sharper and narrower, indicating a larger crystal size and better crystallinity. The EDS analysis shown in Fig. 2(b) clearly demonstrates the presence of Cu and O peaks, and a quantitative analysis reveals that Cu and O are in a 1:1 stiochoimetric ratio. The EDS analysis reconfirms the high purity of the final product with no impurities.

Fig. 3 shows the FT-IR spectra of CuO nanostructures prepared at different hydrothermal temperatures. Three characteristic absorption peaks of CuO positioned at 613, 506 (a Cu–O stretching along [−202] direction), and 419 cm^{-1} (a Cu–O stretching along [202] direction) could be observed. These are the characteristic stretching vibrations of Cu–O bonds in the monoclinic CuO phase [33,34].

Fig. 4 shows a typical SEM image taken from the CuO sample synthesized at 100 °C. The low magnification SEM micrograph gives the overall morphology of CuO nanobelts. The magnified image shows that the nanobelts are relatively straight and long with a length up to 4 μm. The diameter of nanobelts is ranging from 200 to 800 nm.

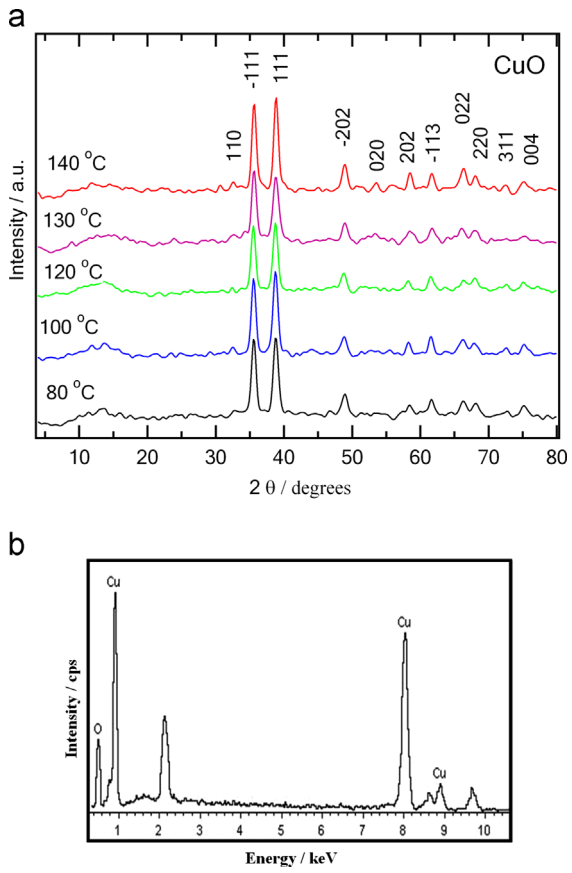

Fig. 2. XRD patterns for CuO nanostructures prepared at different temperatures via a hydrothermal technique (a) and the corresponding EDS chemical analysis for the sample prepared at 140 °C.

The morphology of CuO nanobelts prepared at 100 and 140 °C was further observed with TEM. Fig. 5 presents typical TEM images of the obtained nanobelt-like CuO nanostructures with the SAED pattern depicted in Fig. 5(b). The width and thickness of the nanobelts are not uniform along their entire lengths. The nanobelts shown in Fig. 5(a) indicate that each nanobelt consists of wide stems between 300 and 500 nm with sharp tips ranging in size from 80 to 150 nm. It appears that at an elevated temperature of 140 °C (Fig. 5(b)), the nanobelts are likely agglomerated to each other. It can be also seen that most of the nanobelts have lengths between 2 and 6 μm. The electron diffraction pattern indicates that CuO nanobelts are well crystallized, in good agreement with the XRD results shown in Fig. 2.

3.2. Formation mechanism

Based on the above experimental results, a reaction mechanism of CuO nanobelts synthesized using the current hydrothermal approach is proposed. The copper ions in the precursor can react with ammonia solution to form clear and homogeneous $\{Cu^{2+}$–ammonia:$[Cu(NH_3)_4]^{2+}\}$ complex. Upon the

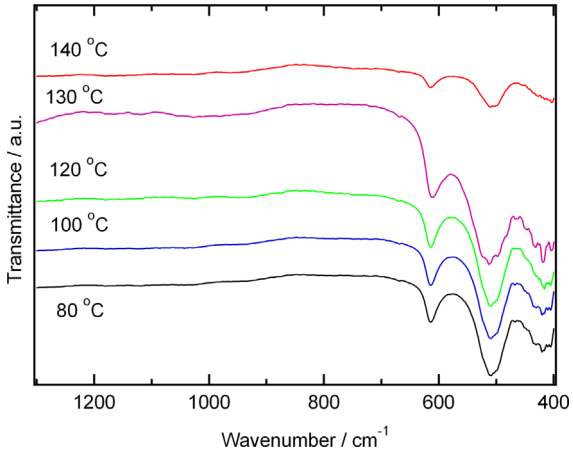

Fig. 3. FT-IR spectra of CuO nanostructures prepared at different hydrothermal temperatures.

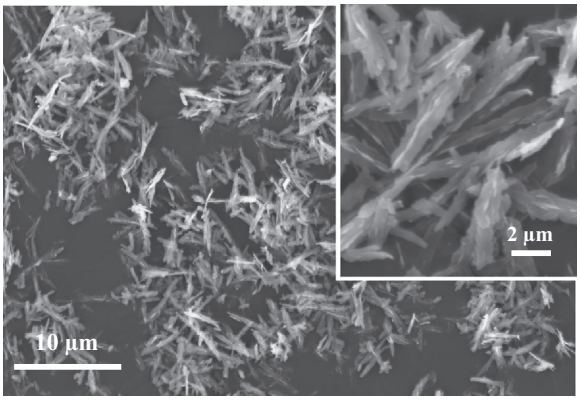

Fig. 4. SEM micrograph of CuO nanobelts corresponding to the sample prepared at a hydrothermal temperature of 100 °C. The inset shows a magnified image of the same sample.

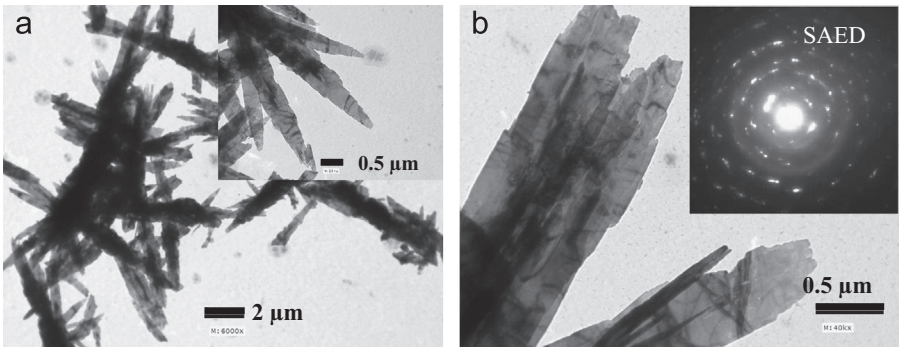

Fig. 5. TEM images of CuO nanobelts prepared at two different hydrothermal temperatures, (a) 100 °C and (b) 140 °C, with SAED pattern depicted in the inset.

addition of the NaOH solution, a blue precipitate of $Cu(OH)_2$ is formed according to the following reaction:

$$Cu^{2+}+2OH^- \rightarrow Cu(OH)_2$$

With the hydrothermal treatment at a desired temperature, CuO could be formed via the thermal dehydration and re-crystallization processes of the pre-existing $Cu(OH)_2$ according to the following equation:

$$Cu(OH)_2 \rightarrow CuO+H_2O$$

A similar observation in an experimental system composed of NH_3/KOH was reported earlier by Lu et al. [35]. The transformation pathway from $Cu(OH)_2$ to CuO has been addressed by Cudennec and Lecert [36]. They suggested that, in the presence of a NaOH alkaline solution, $[Cu(OH)_4]^{2-}$ ions are firstly produced instead of solid $Cu(OH)_2$. Then a condensation process accompanied by a loss of two hydroxyl ions and one water molecule may lead to the formation of CuO [32,36]. Such a transformation process can be described by the following scheme:

$$Cu(OH)_2+2OH^- \rightarrow [Cu(OH)_4]^{2-}$$

$$[Cu(OH)_4]^{2-} \rightarrow CuO+2OH^-+H_2O$$

Under optimal experimental conditions, the initially formed CuO nanoparticles are assembled with oriented growth into nanobelts. The growth to 1D nanostructure is linked to the intrinsic anisotropic property of monoclinic CuO. Consequently, the aggregated nanoparticles tend to arrange themselves and attach to each other to reduce the energy of the system. The presence of water facilitates the morphological transformation to nanobelts. Further studies are needed to completely understand the reaction mechanism.

3.3. Optical and magnetic properties

UV–vis spectroscopy is firstly used to understand the optical absorption properties of CuO nanostructures. Prior to measurement, CuO samples are dispersed in water and ethanol by ultrasonication. The optical absorption spectra in both solutions are almost identical (as shown in Fig. 6). The UV–vis spectra of the CuO samples exhibit a sharp absorption peak at ~286 nm, which is a characteristic peak of monoclinic CuO [37]. A weak, broad absorption peak centered at ~380 nm is attributed to

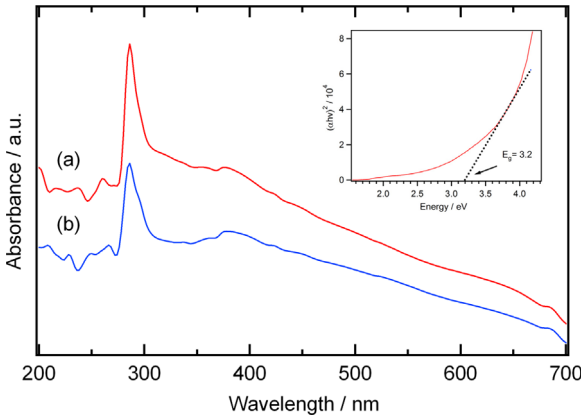

Fig. 6. UV–vis absorption spectra of CuO nanobelts dispersed in (a) ethanol and (b) water. The inset shows $(\alpha h\nu)^2$–$h\nu$ curve for sample (b).

band gap transition of CuO [38]. The optical band gap energy (E_g) was estimated using the following equation [39,40]:

$$(\alpha h\nu)^n = B/(h\nu - E_g),$$

where α is the absorption coefficient, $h\nu$ is the photo energy, B is a material-related constant, and n is either 2 for a direct transition or 1/2 for an indirect transition. The direct band gap energy for CuO was estimated by extrapolating the linear region at the steeply increasing curve of the plot of $(\alpha h\nu)^2$ versus ($h\nu$). The value of the band gap is given by the x-intercept (as shown in the inset of Fig. 6) for the sample dispersed in water. The obtained value was found to be 3.2 eV. A similar value was obtained with the sample dispersed in ethanol. Such a band gap value was larger than the reported value for the bulk CuO (E_g = 1.85 eV) [41]. An increase of optical band gap value to 3.2 eV was also observed and reported for CuO nanorods [42]. Light absorption generates an electron in the conduction band and a positive hole in the valence band. A confinement is expected with small particles, which leads to a quantization of energy levels. Such a phenomenon arises when particle size becomes comparable to the de Broglie wavelength of a charge carrier. The observed widening in the band gap of the CuO nanobelts is indicative of quantum size effects [43].

The room temperature photoluminescence (PL) spectra of as-prepared CuO nanobelts are shown in Fig. 7 after exciting the sample using (λ_{ext} = 320 nm). Three emission peaks are

observed for CuO: a sharp emission peak at 362 nm, a broad emission at 400–500 nm, and a relatively low intensity peak at 725 nm. All of the emission bands' peak wavelengths shown in Fig. 7 were previously reported for CuO [44–46]. The peak at 362 nm corresponds to the band-edge emission [47]. However, the peak position is blue-shifted in comparison to bulk CuO, in agreement with the findings of UV–vis analysis. Due to the presence of nanobelts in the material, a quantum confinement effect is induced, leading to a blue shift in the PL peak position. This result is consistent with a previous report [48]. The peak detected at 725 nm may have been caused by a single ionized oxygen vacancy, resulting in red emission of CuO materials due to a recombination of a photo generated hole with a single ionized electron in the valence band [49,50]. It is worthy to note that, exciting the sample using a higher wavelength (λ_{ext}=470 nm) led to similar PL emission peaks as obtained above.

The magnetic properties of CuO nanobelts synthesized at 100 °C were measured at room temperature (T=298 K) and in liquid nitrogen (T=77 K) and the obtained results are shown in Fig. 8. For the sample measured at T=77 K, Fig. 8(a), a linear magnetic response up to the maximum applied field (4 kOe) with a magnetization of 0.0049 emu/g was observed. For the magnetic loop measured at T=298 K, Fig. 8(b), a coercive force (H_c) was found to be 93.35 Oe, with a 0.1427 emu/g magnetization measured under a maximum field of 12 kOe. These findings clearly demonstrated that CuO nanonbelts exhibit a ferromagnetic behavior at room temperature and a paramagnetic characteristic in liquid nitrogen. The paramagnetic behavior observed at low temperature may be related to the uncompensated Cu^{2+} surface spins. Uncompensated moment may be induced from imbalance in the number of up and down spins due to the spin-structural disorder at the surface of antiferromagnetic material as suggested by Mørup et al. [51] or from the presence of defects like oxygen vacancies [52].

It is worthy to note that, such magnetic behavior of CuO nanobelts depends not only on the material size but also on its shape. In the present study, the size of the CuO nanobelts is quite larger than the critical size of 10 nm of spherical CuO nanoparticles that correspond to weak ferromagnetic behavior [53–55], indicating the crucial role of CuO shape in magnetic behavior. Bulk CuO is a category of antiferromagnetism. The origin of the net magnetic moments of antiferromagnetic CuO nanoparticles is still a matter of investigation due to the presence of complex phenomena related to uncompensated surface spins and size effects [56]. For the same volume, the specific surface area of CuO nanobelts is likely larger than the corresponding nanoparticles. This would lead to more uncompensated surface spins for the CuO nanobelts, which in turn results in more exchange bias. The shape of the hysteresis loop is essentially affected by both surface area and magnetic anisotropy [57]. In contrast to the spherical nanoparticles, the current CuO nanobelts have shape anisotropy, which would result in coercive enhancement. Based on the above explanation, CuO nanobelts are indicated to have a strong influence on ferromagnetic behavior. This observation is in good agreement with the ferromagnetic behavior reported earlier for CuO nanorods [58].

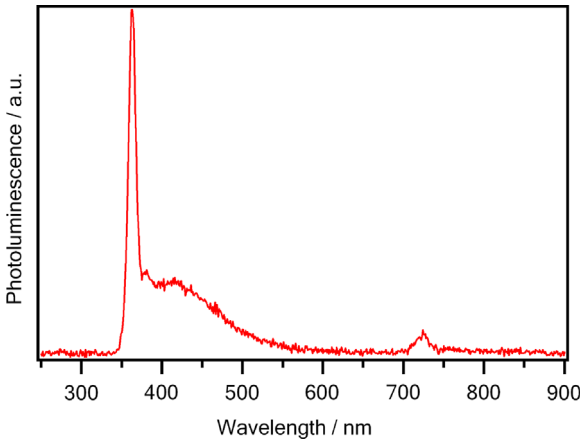

Fig. 7. Photoluminescence (PL) spectra, measured at room temperature, for CuO nanobelts. Excitation source: 150 W xenon lamp.

4. Conclusion

We have demonstrated a simple, convenient hydrothermal route to synthesize CuO nanobelts. The products have been

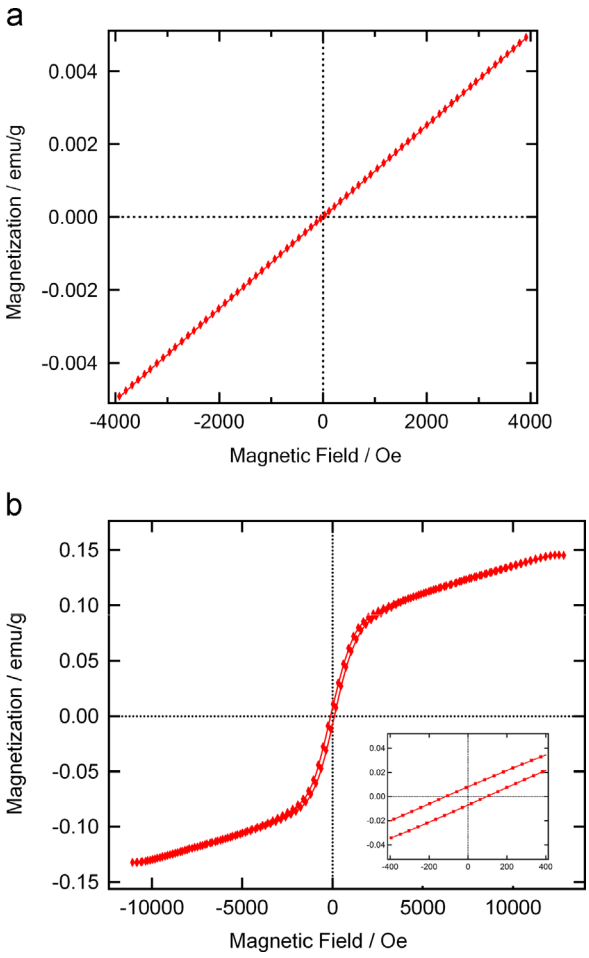

Fig. 8. Magnetic hysteresis behavior (M–H loops) of CuO nanobelts grown at 100 °C hydrothermal temperature. The loops were measured at (a) T=77 K and (b) T=298 K. Inset of (b) shows a magnified narrow section of the loop.

fully characterized using a variety of analytical techniques, including XRD, FT-IR, SEM, EDS, TEM, UV–vis, PL, and VSM. The results indicated the formation of a single monoclinic phase of CuO with nanobelts morphology. A widening of optical band gap energy compared to the bulk CuO was observed and attributed to quantum size effects. Ferromagnetic behavior was achieved at room temperature and was related to the morphology of as-synthesized CuO nanostructures. Such CuO nanobelts are expected to have potential applications in fields such as drug delivery, magnetic resonance imaging, heterogeneous catalysis, and field emission devices.

Acknowledgment

This paper was funded by the Deanship of Scientific Research (DSR), King Abdulaziz University, Jeddah, under Grant number (130-007-D1433). The authors, therefore, acknowledge with thanks DSR technical and financial support.

References

[1] L.-Y. Zhang, D.-S. Xue, X.-F. Xu, A.-B. Gui, Magnetic properties and Verwey transition of quasi-one-dimensional magnetite nanowire arrays assembled in alumina templates, Journal of Magnetism and Magnetic Materials 294 (2005) 10–15.

[2] Y.H. Ogata, A. Koyama, F.A. Harraz, M.S. Salem, T. Sakka, Electrochemical formation of porous silicon with medium sized-pores, Electrochemistry 75 (3) (2007) 270–272.

[3] Y. Xia, P. Yang, Y. Sun, Y. Wu, B. Mayers, B. Gates, Y. Yin, F. Kim, H. Yan, One-dimensional nanostructures: Synthesis, characterization, and applications, Advanced Materials 15 (2003) 353–389.

[4] S.M. El-Sheikh, F.A. Harraz, M.M. Hessien, Magnetic behavior of cobalt ferrite nanowires prepared by template–assisted technique, Materials Chemistry and Physics 123 (2010) 254–259.

[5] J.R. Morber, Y. Ding, M.S. Haluska, Y. Li, J.P. Liu, Z.L. Wang, R.L. Snyder, PLD-assisted VLS growth of aligned ferrite nanorods, nanowires, and nanobelts synthesis, and properties, Journal of Physical Chemistry B 110 (2006) 21672–21679.

[6] R.M. Mohamed, M.M. Rashad, F.A. Harraz, W. Sigmund, Structure and magnetic properties of nano-crystalline cobalt ferrite powders synthesized using organic acid precursor method, Journal of Magnetism and Magnetic Materials 322 (2010) 2058–2064.

[7] X. Wang, Y.D. Li, Synthesis and formation mechanism of manganese dioxide nanowires/nanorods, Chemistry—A European Journal 9 (2003) 300–306.

[8] M. El-Sheikh, F.A. Harraz, K.A. Saad, Catalytic performance of nanostructured iron oxides synthesized by thermal decomposition technique, Journal of Alloys and Compounds 487 (2009) 716–723.

[9] F.A. Harraz, R.M. Mohamed, A. Shawky, I.A. Ibrahim, Composition and phase control of Ni/NiO nanoparticles for photocatalytic degradation of EDTA, Journal of Alloys and Compounds 508 (2010) 133–140.

[10] J.P. Jolivet, S. Cassaignon, C. Chaneac, D. Chiche, E. Tronc, Design of oxide nanoparticles by aqueous chemistry, Journal of Sol–Gel Science and Technology 46 (2008) 299–305.

[11] A.Q. Musa, T. Akomolafe, M.J. Carter, Production of cuprous oxide, a solar cell material, by thermal oxidation and a study of its physical and electrical properties, Solar Energy Materials and Solar Cells 51 (1998) 305–316.

[12] L. Liao, Z. Zhang, B. Yan, Z. Zheng, Q.L. Bao, T. Wu, C.M. Li, Z.X. Shen, J.X. Zhang, H. Gong, J.C. Li, T. Yu, Multifunctional CuO nanowire devices: p-type field effect transistors and CO gas sensors, Nanotechnology 20 (2009) 085203–085208.

[13] B. Balamurugan, B.R. Mehta, D.K. Avasthi, F. Singh, A.K. Arora, M. Rajalakshmi, G. Raghavan, A.K. Tyagi, S.M. Sivaprasad, Modifying the nanocrystalline characteristics structure, size, and surface states of copper oxide thin films by high-energy heavy-ion irradiation, Journal of Applied Physics 92 (2002) 3304–3310.

[14] G. Avgouropoulos, T. Ioannides, C. Papadopoulou, J. Batista, S. Hocevar, H.K. Matralis, A comparative study of Pt/γ-Al_2O_3, Au/α-Fe_2O_3 and CuO–CeO_2 catalysts for the selective oxidation of carbon monoxide in excess hydrogen, Catalysis Today 75 (2002) 157–167.

[15] R.A. Borzi, S.J. Stewart, R.C. Mercad er, G. Punte, F. Garcia, Magnetic behavior of nanosized cupric oxide, Journal of Magnetism and Magnetic Materials 226–230 (2001) 1513–1515.

[16] H. Eskes, L.H. Tjeng, G.A. Sawatzky, Cluster-model calculation of the electronic structure of CuO: a model material for the high-T_c superconductors, Physical Review B 41 (1990) 288–299.

[17] A.H. MacDonald, Superconductivity: copper oxides get charged up, Nature 414 (2001) 409.

[18] X.P. Gao, J.L. Bao, G.L. Pan, H.Y. Zhu, P.X. Huang, F. Wu, D.Y. Song, Preparation and electrochemical performance of polycrystalline and single crystalline CuO nanorods as anode materials for Li ion battery, Journal of Physical Chemistry B 108 (2004) 5547–5551.

[19] X. Zhang, G. Wanga, X. Liua, H. Wu, Synthesis and electrochemical properties of CuO nanobelts, Materials Chemistry and Physics 112 (2008) 726–729.

[20] H. Zhang, M. Zhang, Synthesis of CuO nanocrystalline and their application as electrode materials for capacitors, Materials Chemistry and Physics 108 (2008) 184–187.

[21] X.G. Zheng, C.N. Xu, Y. Tomokiyo, E. Tanaka, H. Yamada, Y. Soejima, Observation of charge stripes in cupric oxide, Physical Review Letters 85 (2000) 5170–5173.

[22] K. Borgohain, S.J. Mahamuni, Formation of single-phase CuO quantum particles, Journal of Materials Research 17 (2002) 1220–1223.

[23] Z. Yang, J. Xu, W. Zhang, A. Liu, S. Tang, Controlled synthesis of CuO nanostructures by a simple solution route, Journal of Solid State Chemistry 180 (2007) 1390–1396.

[24] Z.W. Pan, Z.R. Dai, Z.L. Wang, Nanobelts of semiconducting oxides, Science 291 (2001) 1947–1949.

[25] H. Ming, K. Pan, Y. Liu, H. Li, X. He, J. Ming, Z. Ma, Z. Kang, Electrochemical fabrication of $Cu(OH)_2$ and CuO nanostructures and their catalytic property, Journal of Crystal Growth 327 (2011) 251–257.

[26] M. Samy El-Shall, W. Slack, W. Vann, D. Kane, D. Hanley, Synthesis of nanoscale metal oxide particles using laser vaporization/condensation in a diffusion cloud chamber, Journal of Physical Chemistry 98 (12) (1994) 3067–3070.

[27] H.T. Zhu, C.Y. Zhang, Y.M. Tang, J.X. Wang, Novel synthesis and thermal conductivity of CuO nanofluid, Journal of Physical Chemistry C 111 (2007) 1646–1650.

[28] Y. Liu, Y. Chu, Y. Zhuo, M. Li, L. Li, L. Dong, Anion-controlled construction of CuO honeycombs and flowerlike assemblies on copper foils, Crystal Growth and Design 7 (2007) 467–470.

[29] F.A. Harraz, Polyethylene glycol-assisted hydrothermal growth of magnetite nanowires: synthesis and magnetic properties, Physica E: Low-Dimensional Systems and Nanostructures 40 (2008) 3131–3136.

[30] R.M. Mohamed, F.A. Harraz, I.A. Mkhalid, Hydrothermal synthesis of size controllable Yttrium Orthovanadate (YVO_4) nanoparticles and its application in photocatalytic degradation of direct blue dye, Journal of Alloys and Compounds 532 (2012) 55–60.

[31] D. Chen, G.Z. Shen, K.B. Tang, Y.T. Qian, Large-scale synthesis of CuO shuttle-like crystals via a convenient hydrothermal decomposition route, Journal of Crystal Growth 254 (2003) 225–228.

[32] G.H. Du, V. Tendeloo, $Cu(OH)_2$ nanowires, CuO nanowires and CuO nanobelts, Chemical Physics Letters 393 (2004) 64–69.

[33] M. Zhang, X. Xu, M. Zhang, Hydrothermal synthesis of sheaf-like CuO via ionic liquids, Materials Letters 62 (2008) 385–388.

[34] Y.Y Xu, D.R. Chen, X.L. Jiao, Fabrication of CuO pricky microspheres with tunable size by a simple solution route, Journal of Physical Chemistry B 109 (2005) 13561–13566.

[35] C.H. Lu, L.M. Qu, J.H. Yang, D.Y. Zhang, N.Z. Wu, J.M. Ma, Simple template-free solution route for the controlled synthesis of $Cu(OH)_2$ and

CuO nanostructures, Journal of Physical Chemistry B 108 (2004) 17825–17831.
[36] Y. Cudennec, A. Lecert, The transformation of $Cu(OH)_2$ into CuO, revisited, Solid State Sciences 5 (2003) 1471–1474.
[37] N. Topnani, S. Kushwaha, T. Athar, Wet synthesis of copper oxide nanopowder, International Journal of Green Nanotechnology: Materials Science and Engineering 1 (2009) M67–73.
[38] J. Wang, S. He, Z. Li, X. Jing, M. Zhang, Z. Jiang, Self-assembled CuO nanoarchitectures and their catalytic activity in the thermal decomposition of ammonium perchlorate, Colloid and Polymer Science 287 (2009) 853–858.
[39] J. Pankove, Optical Processes in Semiconductors, Prentice-Hall, Englewood Cliffs, New Jersey, 1979.
[40] K.F. Shan, I.B. Kim, X.G. Liu, F.Z. Liu, Y.J. Sohn, J.W. Lee, Blueshift of near band edge emission in Mg doped ZnO thin films and aging, Journal of Applied Physics 95 (2004) 4772–4776.
[41] H. Wang, J.Z. Xu, J.J. Zhu, H.Y. Chen, Preparation of CuO nanoparticles by microwave irradiation, Journal of Crystal Growth 244 (2002) 88–94.
[42] Q. Liu, Y. Liang, H. Liu, J. Hong, Z. Xu, Solution phase synthesis of CuO nanorods, Materials Chemistry and Physics 98 (2006) 519–522.
[43] J.P. Yang, F.C. Meldrum, J.H. Fendler, Epitaxial growth of size-quantized cadmium sulfide crystals under arachidic acid monolayers, Journal of Physical Chemistry 99 (1995) 5500–5504.
[44] C. Jin, K. Baek, S. Park, H.W. Kim, W.I. Lee, C. Lee, Influence of SnO_2 coating and thermal annealing on the structure and luminescence properties of CuO nanorods, Solid State Communications 150 (2010) 1812–1815.
[45] B. Toboonsung, P. Singjai, Formation of CuO nanorods and their bundles by an electrochemical dissolution and deposition process, Journal of Alloys and Compounds 509 (2011) 4132–4137.
[46] R. Al-Gaashani, S. Radiman, N. Tabet, A. Razak Daud, Synthesis and optical properties of CuO nanostructures obtained via a novel thermal decomposition method, Journal of Alloys and Compounds 509 (2011) 8761–8769.
[47] L.R. Singh, R.S. Ningthoujam, V. Sudarsan, S.D. Singh, S.K. Kulshreshtha, Probing of surface Eu^{3+} ions present in ZnO:Eu nanoparticles by covering ZnO:Eu core with Y_2O_3 shell: luminescence study, Journal of Luminescence 128 (2008) 1544–1550.
[48] S.K. Maji, N. Mukherjee, A. Mondal, B. Adhikary, B. Karmakar, Chemical synthesis of mesoporous CuO from a single precursor: structural, optical and electrical properties, Journal of Solid State Chemistry 183 (2010) 1900–1904.
[49] K. Vanheusden, W.L. Warren, C.H. Seager, D.R. Tallant, J.A. Voigt, B.E. Gnade, Mechanisms behind green photoluminescence in ZnO phosphor powders, Journal of Applied Physics 79 (1996) 7983–7990.
[50] R.S. Ningthoujam, N.S. Gajbhiye, A. Ahmed, S.S. Umre, S.J. Sharma, Re-dispersible Li^+ and Eu^{3+} Co-doped nanocrystalline ZnO: luminescence and EPR studies, Journal of Nanoscience and Nanotechnology 8 (2008) 3059–3062.
[51] S. Mørup, D.E. Madsen, C. Frandsen, C.R.H. Bahl, M.F. Hansen, Experimental and theoretical studies of nanoparticles of antiferromagnetic materials, Journal of Physics: Condensed Matter 19 (2007) 213202–213232.
[52] S. Rehman, A. Mumtaz, S.K. Hasanain, Size effects on the magnetic and optical properties of CuO nanoparticles, Journal of Nanoparticle Research 13 (2011) 2497–2507.
[53] A. Punnoose, H. Magnone, M.S. Seehra, Bulk to nanoscale magnetism and exchange bias in CuO nanoparticles, Physical Review B 64 (2001) 174420–174427.
[54] X.G. Zheng, T. Mori, K. Nishiyama, W. Higemoto, C.N. Xu, Dramatic suppression of antiferromagnetic coupling in nanoparticle CuO, Solid State Communications 132 (2004) 493–496.
[55] T. Ahmad, R. Chopra, K.V. Ramanujachary, S.E. Lofland, A.K. Ganguli, Canted antiferromagnetism in copper oxide nanoparticles synthesized by the reverse-micellar route, Solid State Sciences 7 (2005) 891–895.
[56] G. Narsinga Rao, Y.D. Yao, J.W. Chen, Superparamagnetic behavior of antiferromagnetic CuO nanoparticles, IEEE Transactions on Magnetics 41 (2005) 3409–3411.
[57] B.D. Cullity, in: M. Cohen (Ed.), Introduction to Magnetic Materials, Addison-Wesley, Reading, MA, 1972, pp. 240–243.
[58] H.-M. Xiao, L.-P. Zhu, X.-M. Liu, S.-Y. Fu, Anomalous ferromagnetic behavior of CuO nanorods synthesized via hydrothermal method, Solid State Communications 141 (2007) 431–435.